Phase and film formation pathway for vacuum-deposited $Cu_2BaSn(S, Se)_4$ absorber layers

Jon-Paul Sun,[1] José A. Márquez,[2] Helena Stange,[3] Roland Mainz,[2] and David B. Mitzi[1,4]
[1]*Department of Mechanical Engineering and Materials Science, Duke University, Durham, North Carolina 27708, USA*
[2]*Helmholtz-Zentrum Berlin für Materialien und Energie GmbH, Hahn-Meitner-Platz 1, 14109 Berlin, Germany*
[3]*Technische Universität Berlin, Institut für Werkstoffwissenschaften, Ernst-Reuter Platz 1, 10587 Berlin, Germany*
[4]*Department of Chemistry, Duke University, Durham, North Carolina 27708, USA*

(Received 9 March 2019; published 15 May 2019)

Earth-abundant copper barium thioselenostannate, $Cu_2BaSn(S, Se)_4$, absorbers have recently demonstrated promising optoelectronic and defect resistance properties for solar harvesting applications. The highest photovoltaic device efficiencies have been achieved in vacuum-based co-sputter deposited films, yet there is a tendency for a multilayer formation consisting of large, plateletlike surface grains and a smaller grain-sized underlayer (often accompanied by voids). In this work we use a combination of *in situ* and *ex situ* x-ray diffraction and scanning electron microscopy to unravel the coupling of phase evolution to film morphology. We find that Cu surface migration and associated Cu-rich phases play a defining role in determining the overall film structure.

DOI: 10.1103/PhysRevMaterials.3.055402

I. INTRODUCTION

The progress in thin-film chalcogenide photovoltaics (PVs) has been exemplified by the already-commercialized CdTe and $Cu(In, Ga)(S, Se)_2$ (CIGSSe) technologies, achieving power conversion efficiencies (PCEs) in excess of 20% [1]. Yet Cd toxicity concerns aside, the low reserve base of In and Te present formidable barriers to terawatt-scale deployment [2,3]. $Cu_2ZnSn(S, Se)_4$ (CZTSSe), in which the In and Ga have been replaced by earth-abundant Zn and Sn, has therefore received significant attention as a potential replacement for CdTe/CIGSSe. However, the record PCE (12.6%) has remained stagnant since 2014 [4], with recent studies pointing to antisite disorder-induced band tailing and deep defects as limiting factors in device performance [5–8]. Designing defect resistance into multinary semiconductors has been proposed through introducing cation size and coordination discrepancy [9–13]. In CZTSSe, the Cu^+ and Zn^{2+} ions share the same tetrahedral coordination and ionic size (~0.6 Å) [14]. By replacing Zn^{2+} with Ba^{2+} in $Cu_2BaSn(S, Se)_4$ (CBTSSe), the larger Ba^{2+} ion (1.42 Å) [14] adopts an eightfold coordination, which is expected to increase potential barriers to antisite formation [12,13].

CBTSSe has recently shown promising performance in both PV [9,15–19] and photoelectrochemical (PEC) [15,20–24] devices, achieving 5% PCE and 12 mA cm^{-2} at zero voltage vs the reversible hydrogen electrode (V_{RHE}), respectively. Significantly reduced band tailing compared to CZTSSe is evident from sharper cutoffs in quantum efficiency (QE) response at long wavelengths, in addition to a narrower full-width-at-half-maximum (FWHM) photoluminescence (PL) peak (CBTSSe, 60 nm; CZTSSe, 190 nm) [5,18]. To achieve this performance, Shin *et al.* developed a two-step process, consisting of a vacuum-based precursor (Cu, BaS, Sn) co-sputter deposition, followed by annealing under S to convert to Cu_2BaSnS_4 (CBTS), with a subsequent annealing under Se to partially substitute S atoms. As Se is incorporated into $Cu_2BaSnS_{4-x}Se_x$, the band gap (E_g) decreases from 2.03 ($x = 0$) to 1.55 eV ($x = 3$), within the optimal range for single-junction PV (1.0–1.6 eV) [18].

Despite the promising defect resistance and optical properties of CBTSSe, significant progress needs to be made before it can be considered for commercialization. The open circuit voltage (V_{oc}) of the best device reached 610 mV, representing a V_{oc} deficit ($E_g/q - V_{oc}$) of 940 mV [18]. Considering the sharp QE cutoff, this suggests either the band alignment of the commonly used CdS buffer layer may not be optimal for this material, or alternatively the absorber is plagued by recombination losses. In nonselenized CBTS, Ge *et al.* oxygenated the CdS buffer layer to lower the electron affinity and improve V_{oc} by 450 mV, suggesting a clifflike interface between CBTS and CdS may be hindering performance [16]. Future studies should investigate the effects of stoichiometry on carrier concentrations and lifetimes—both critical parameters for optimizing absorber and device performance. In CZTSSe, formation under low-Cu and high-Zn conditions has been found to be beneficial due to low formation energies of both V_{Cu} (shallow acceptor) and $[2Cu_{Zn} + Sn_{Zn}]$ (Sn_{Zn} is a deep donor) defect clusters [25–30]. Due to the similar nature of the valence band, V_{Cu} is also expected to be a shallow acceptor in CBTSSe, although issues with Cu_{Ba} and Sn_{Ba} antisite formation are not expected to be prevalent in this system [12,13]. However, a more pressing issue to resolve is an understanding of the morphology formation of the active layer. In cross-section scanning electron microscopy (SEM) images presented by Shin *et al.*, the films show a distinct two-layer organization. The upper half of the film is composed of ~2-μm flat grains, while the lower half is composed of a smaller grain-sizes layer containing multiple voids [18].

Since the performance of a PV device is strongly tied to the underlying film morphology, we decided to understand the film growth mechanisms before attempting to tune the remaining dependent areas of concern. In this report we use a combination of *in situ* and *ex situ* x-ray diffraction (XRD)

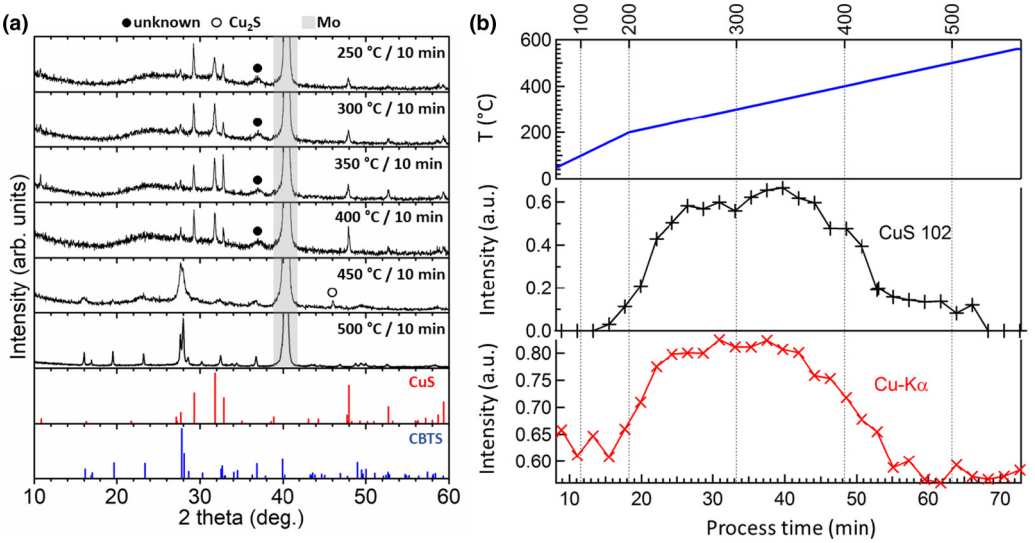

FIG. 1. (a) XRD patterns of films annealed under S at various temperatures, with standards for CuS [Joint Committee on Powder Diffraction Standards (JCPDS) 6–464] and CBTS (JCPDS 30–124) shown at the bottom and (b) *in situ* EDXRD intensity of the CuS 102 scattering peak (middle panel), Cu $K\alpha$ fluorescence (bottom), and temperature profile (top) of a precursor film under S.

in combination with SEM to understand the film growth mechanisms of co-sputter-deposited CBTSSe films. The understanding gained in this study is also expected to provide insights for the deposition of other Cu-containing multinary chalcogenides.

II. EXPERIMENT

Thin films were deposited onto Mo-coated glass substrates (Thin Film Devices) via RF magnetron co-sputtering from Cu, BaS, and Sn targets (AJA), as described in detail by Shin *et al.* [18]. Films were converted to the desired phases by annealing in either S or Se vapor under a quartz cover, within a N_2-filled glovebox. *Ex situ* XRD spectra were collected using a PANalytical Empyrean diffractometer with Cu $K\alpha$ radiation under ambient conditions. *In situ* energy-dispersive x-ray diffraction (EDXRD) and fluorescence data were collected in real time during sulfurization at the EDDI beamline [31] of the BESSY II synchrotron facility [32] by an energy-dispersive high-purity Ge detector. As opposed to conventional XRD where the excitation energy is fixed while the scattering angle is scanned, in EDXRD the scattering angle is fixed while the excitation energy is scanned. For the sulfurizations, the samples were heated with sulfur flakes in a cylindrical graphite reaction box with quartz top and bottom lids placed inside a vacuum chamber with a base pressure of $\sim 10^{-4}$ mbar. The atmosphere of the reaction box is decoupled from that of the vacuum chamber by a motor valve before heating. Samples and sulfur flakes are heated by the radiation of four halogen lamps each above and below the reaction box with a total power of 4 kW. Further details can be found in Ref. [33]. SEM secondary electron images were collected using a combination of FEI XL30 SEM-FEG, FEI Apreo S, and Hitachi S-4700 instruments, with accelerating voltages of 2 kV and 25-pA probe currents. Energy-dispersive spectroscopy (EDS) images were collected on an FEI Apreo S instrument, with an accelerating voltage of 10 kV and a 50-pA probe current. For the EDS measurements, 10 nm of Au were deposited onto samples to improve signal quality. X-ray photoelectron spectroscopy (XPS) was performed using a Kratos Analytical Axis Ultra with monochromated Al $K\alpha$ radiation.

III. RESULTS

A. Cu migration and phase evolution

To understand the film growth process, co-sputter-deposited precursor films with stoichiometric amounts of Cu, BaS, and Sn (2:1:1) were annealed under S for 10 min at various temperatures, so that the phase evolution could be tracked. Figure 1(a) shows the XRD patterns as the films are subjected to increasing temperatures. Between 250 °C and 400 °C, the dominant crystalline phase present is CuS. The broad peak at 37° (●) could not be uniquely assigned. At 450 °C, CuS reduces to Cu_2S while CBTS also begins to form. By 500 °C, CBTS has fully formed and crystallized. Cross-section SEM images (Fig. 2) reveal that new crystallites form on top of the precursor film, suggesting that CuS predominantly forms on the surface of the films, implying that Cu atoms migrate to the surface over short time scales. The presence of a Cu-rich layer on top of the films is supported by elemental mapping of SEM images using EDS (Fig. 3), showing the surface rich in Cu while the bulk of the film contains more Ba and Sn. To further confirm this hypothesis, *in situ* EDXRD was used to monitor the evolution of the CuS 102 reflection peak [corresponding to $2\theta = 29.3°$ in Fig. 1(a)], as well as the Cu $K\alpha$ fluorescence, as a precursor sample was subjected to a continuous temperature ramp under S [Fig. 1(b)]. In close agreement with the *ex situ* data, the intensity of the CuS reflection peak begins to increase at ∼200 °C and has significantly decreased by 450 °C. Additionally, the Cu $K\alpha$ fluorescence intensity closely follows the CuS 102 peak intensity, consistent with the notion that Cu atoms are migrating to the surface where the primary

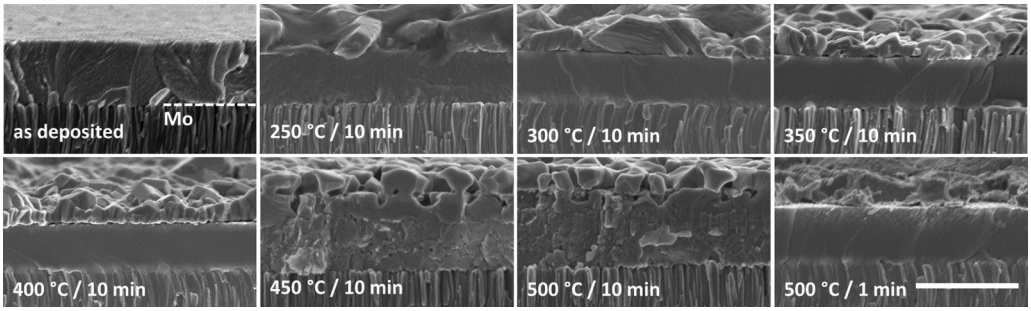

FIG. 2. Cross-section SEM images of films annealed under S for various temperatures and times (scale bar, 1 μm).

fluorescence does not experience as many reabsorption events as it exits the film [34]. XPS spectra of the as-deposited and sulfurized films (Fig. S1 of the Supplemental Material [35]) additionally show that at low annealing temperatures, Ba and Sn are absent from the surface and Cu spectra show an oxidative shift consistent with CuS. To demonstrate that the observed Cu migration is not an artifact of annealing at lower temperatures for extended times, an additional precursor film was annealed at 500 °C for 1 min (Fig. 2, bottom right panel), showing a remarkably similar film structure to those annealed at 250–400 °C for 10 min. This indicates that the phase evolution during device fabrication is appropriately represented by the *ex situ* and *in situ* studies presented.

At 500 °C, the films are single-phase CBTS and well crystallized. The decrease in Cu $K\alpha$ fluorescence indicates that much of the accumulated Cu at the surface has redistributed to the bulk. However, the phase evolution and vertical migration of ions has left a lasting imprint on the film morphology. A close examination of the grain structure of CBTS films [Figs. 4(a) and 4(c)] shows 200–300-nm-diam plateletlike grains on the surface with smaller grains below. During the Se annealing step this two-layer morphology becomes accentuated, with the surface plateletlike grains growing to the micrometer scale [Figs. 4(b) and 4(d)]. The upper layer appears to grow at the expense of the lower, consuming the smaller polycrystalline grains and leaving behind voids, which can lead to shunt paths in devices. We also expect a discrepancy in electronic properties for the upper and lower regions of the film due to the disparity in grain size. The film structures shown in Fig. 4 are typical of co-sputter-deposited films where Cu, BaS, and Sn targets were used [9,18,23], as well as those that used a SnS target in place of Sn [15–17].

Cu surface migration is not a unique phenomenon in CBTSSe. *In situ* studies of the related kesterite system CZTSSe, where Cu-Zn-Sn-S nanoparticle films were heated under Se, have shown that Cu atoms migrate to the surface and form large grains of CuSe and $Cu_{2-x}Se$. The surface grains then expand downwards, incorporating Sn and Zn atoms to form CZTSSe at approximately 350 °C (whereas CBTSSe forms at ∼450 °C) [36,37]. The mechanistic differences between these two systems may lie in the crystal structures of the quaternary species. CZTSSe, $Cu_{2-x}Se$, and the suspected intermediate phases ZnSe and Cu_2SnSe_3 all have essentially cubic close-packed structures with similar underlying lattice constants. This opens up the possibility of topotactic exchange of cations through the S/Se sublattice [36,38]. A similar conclusion has been reached in the formation of $Cu(In, Ga)Se_2$ (CIGSe) via the three-stage co-evaporation process. During the Cu-rich second stage of growth, $Cu_{2-x}Se$ formation has been observed to play a decisive role in large grain formation through a similar topotactic cation exchange mechanism

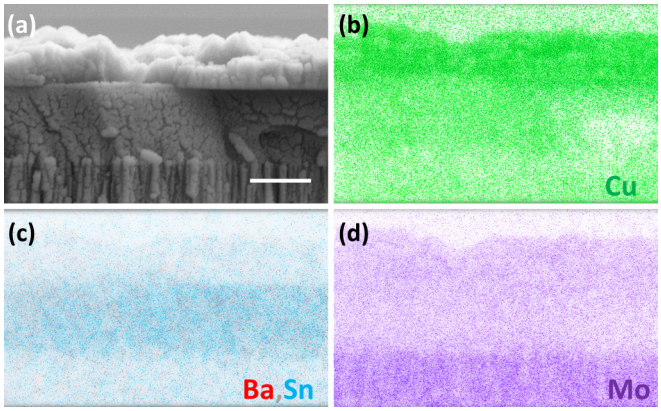

FIG. 3. (a) Cross-section SEM image with EDS mapping of (b) Cu ($L\alpha$, 0.930 keV), (c) Ba ($L\alpha$, 4.465 keV) and Sn ($L\alpha$, 3.443 keV), and (d) Mo ($L\alpha$, 2.293 keV) for a film annealed at 250 °C for 10 min under S (scale bar, 1 μm). Note that the Mo plot contains contributions from S ($K\alpha$, 2.307 keV) due to peak overlap.

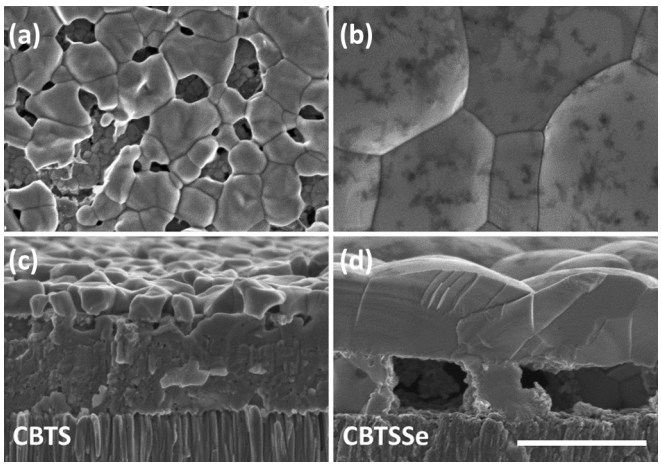

FIG. 4. SEM plan-view (top) and cross-section (bottom) images of films of (a), (c) CBTS annealed at 500 °C under S for 10 min and (b), (d) CBTSSe annealed at 570 °C under Se for 10 min (scale bar for all panels, 1 μm).

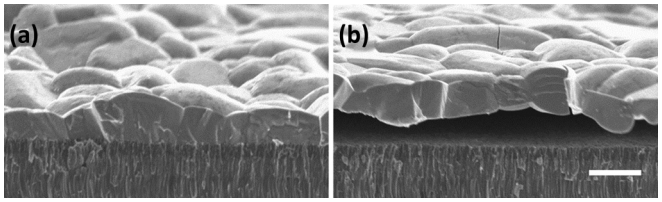

FIG. 5. (a), (b) SEM images of two representative locations of the CBTSSe film formed from a BaS/Sn/Cu precursor stack (scale bar, 1 μm). Image (b) shows the presence of blistering.

[39]. CBTS, however, has a hexagonal crystal structure with eightfold coordinated Ba atoms. In this case it is unclear what role CuS or $Cu_{2-x}S$ has in the formation of the quaternary species. A more rigorous *in situ* study is required to ascertain the detailed phase evolution of this material.

B. Alternative deposition strategies: Cu deposited on top

Given the two-layer morphology of the CBTS films, yet the apparent phase purity when analyzed via XRD, we postulate that CBTS simultaneously forms both at the surface and in the bulk. Differences in morphology could be due to the high S and Cu concentrations at the surface relative to the bulk, and surface energy changes at the solid/gas interface. Regardless of the mechanism, it is plausible that a single-layered film comprised of the large-grained morphology of the surface could be achieved if the Cu is intentionally placed at the surface, thus eliminating CBTS nucleation near the back contact where the small-grain morphology is found. To test this hypothesis, we deposited stacked precursor layers (as opposed to previous co-deposition) with the order BaS/Sn/Cu (Cu on top). Precursor films annealed under S at 450 °C required 3 h to form single-phase CBTS to accommodate the migration times of the precursors. We note that at 500 °C there is no significant difference in required annealing time to form single-phase CBTS. The same 10-min anneal at 570 °C under Se was used to form CBTSSe. Figure 5 shows the resulting CBTSSe film formed using the stacked precursor method. In Fig. 5(a) it is evident that the porous polycrystalline layer (Fig. 4) is absent. The film has adopted the large-grained morphology that we previously attributed to Cu surface migration. However, the film structure now suffers from blistering [Fig. 5(b)].

The blistering originates during the sulfurization step and can first be observed at temperatures near 300 °C (fully formed CBTS films exhibiting blistering are shown in Fig. S2 of the Supplemental Material [35]). Figure 6(a) shows a SEM image of the precursor stack annealed under S at 300 °C. In all examined locations where blistering occurred, the blister cavity formed between the BaS layer and the Mo substrate. The XRD patterns [Fig. 6(b)] reveal that at 300 °C the BaS layer incorporates two additional molar equivalents of S to form BaS_3, undergoing an approximate 150% volume expansion (BaS, 65 $Å^3$/Ba; BaS_3, 97 $Å^3$/Ba) [40,41]. During in-plane expansion while remaining attached to the substrate, blistering is expected to result as a mechanism for relieving stress. Similar blistering has not been noted in stacked precursor CZTSSe films, which can be expected since higher-S-content phases of ZnS are not known to form (except under high pressure) [42]. In the stacked precursor films, we also see evidence for SnS and SnS_2 prior to CBTS formation. In the co-sputter-deposited films, it is likely that these binary species are present but have low crystallinity and are not detectable with standard XRD techniques.

C. Alternative deposition strategies: Increased sulfurization time

A question arises from the above experiment as to whether the long sulfur anneal time at 450 °C might be the dominant cause for the resulting single layer with large grains. To address this question, we investigate the effect of longer anneal times on the morphology of co-sputter-deposited films. Figure 7(a) shows the SEM cross-section images of a co-sputter-deposited film that has been annealed at 450 °C for 3 h under S, and the corresponding CBTSSe film that has been subsequently annealed at 570 °C for 10 min under Se. In the CBTS film, the surface layer has been significantly diminished relative to films that were sulfur annealed for shorter times (i.e., compare with SEM image in Fig. 2). This suggests that the underlying bulk layer is thermodynamically favored during the lower-temperature S anneal and can reabsorb the surface layer given enough time, with the implication that the

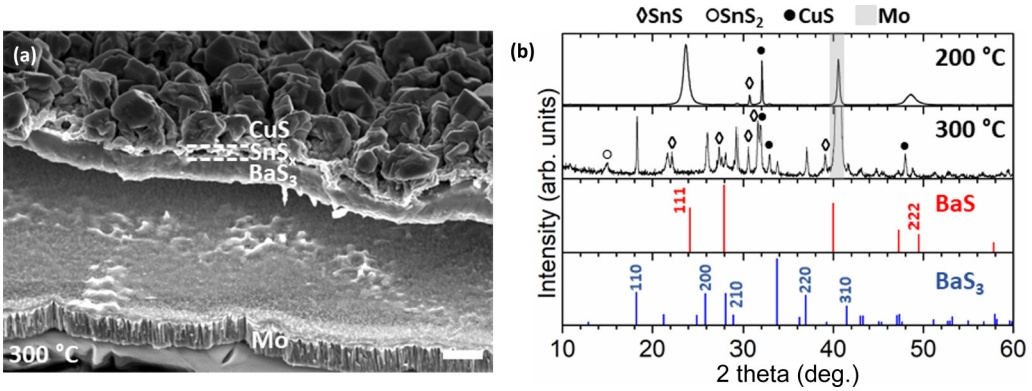

FIG. 6. (a) SEM image showing blister cavity formed between Mo and BaS_3 layers of BaS/Sn/Cu precursor stack sulfurized at 300 °C (scale bar, 1 μm); (b) XRD patterns of BaS/Sn/Cu precursor stack sulfurized at 200 °C and 300 °C, with standards for BaS (JCPDS 8–454) and BaS_3 (JCPDS 1-85-1702).

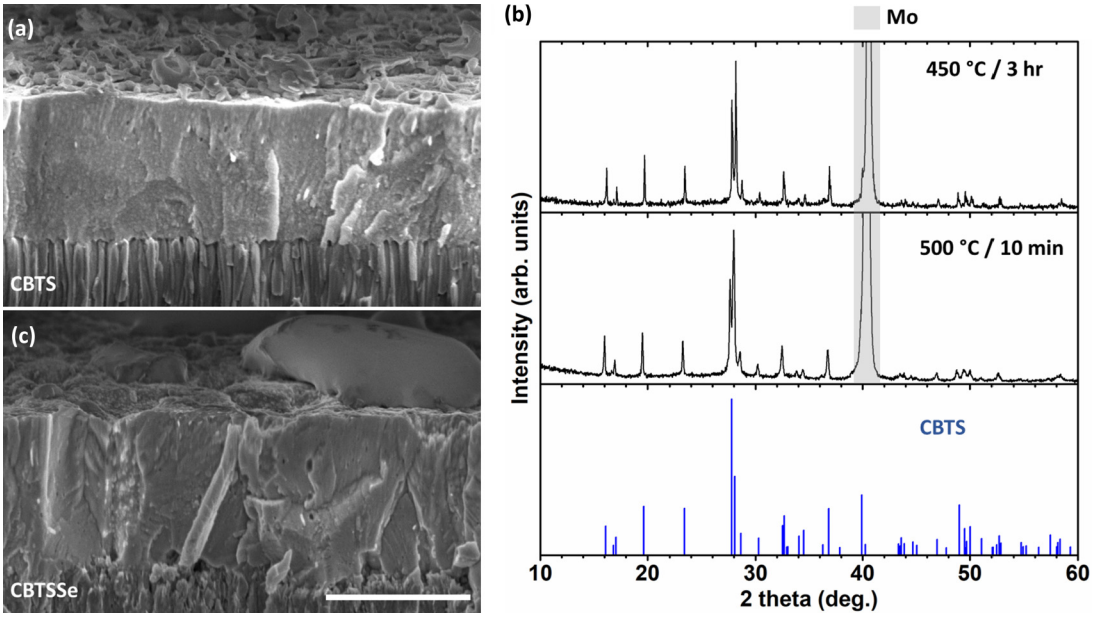

FIG. 7. SEM images of films of (a) CBTS annealed at 450 °C under S for 3 h and (c) CBTSSe subsequently annealed at 570 °C under Se for 10 min (scale bar, 1 μm), both showing a reduction in surface grains compared to CBTS and CBTSSe where 10-min sulfurizations were used. (b) XRD patterns of co-sputter-deposited films annealed under S at the indicated temperatures and times showing single-phase CBTS, with CBTS standard (JCPDS 30–124).

surface atoms are sufficiently mobile for this to occur. In the CBTSSe films, the morphology seen in the CBTS films has largely been retained; however, a sparse layer of the former surface grain morphology is present and may result from the remaining surface crust on the CBTS films. We also note that after a long annealing time the CBTS films are still single phase [Fig. 7(b)] and do not show any change in preferential orientation with respect to films annealed for shorter time—e.g., 500 °C for 10 min.

D. Alternative deposition strategies: Inhibited Cu migration

Finally, we examine the case where CBTS/CBTSSe is formed in the limit where Cu surface migration is strongly inhibited. To achieve this, we first deposited single layers of Sn followed by Cu and annealed under S at 450 °C for 40 min to form Cu_2SnS_3, such that the Cu is bound to a ternary species and has a lower chance of migration. We then deposited a neat layer of BaS on top of the Cu_2SnS_3 and annealed for an additional 3 h at 450 °C under either S or Se to form CBTS or CBTSSe. Since the "precursor" films start out with a high S content, it is possible to directly selenize them without increasing the Se/S ratio above 3 ($CBTS_{1-x}Se_x$ undergoes a phase transition from $P3_1$ to $Ama2$ for $x > 3$) [9]. Figure 8 shows the cross-section SEM images of the CBTS and CBTSSe films formed using this method. Both films adopt a polycrystalline morphology, absent the large surface grains observed in Figs. 4 and 5. This shows that the surface grain morphology can be prevented when the mobility of Cu atoms is reduced and migration to the surface is impeded. It is also interesting to note that the grain size is significantly larger than the bottom layer of films where Cu migration is significant (Fig. 4). At least for the three cases examined in this study (Cu-poor bottom layer, inhibited Cu migration, and Cu-rich surface due to Cu migration) there is a correlation of larger grain size with higher local Cu content. There is also a secondary phase present on the surface of each film. The XRD patterns do not indicate any crystalline secondary phases present; however, we performed XPS (Fig. 9) and observed that the Ba and Sn core levels each have high-binding-energy

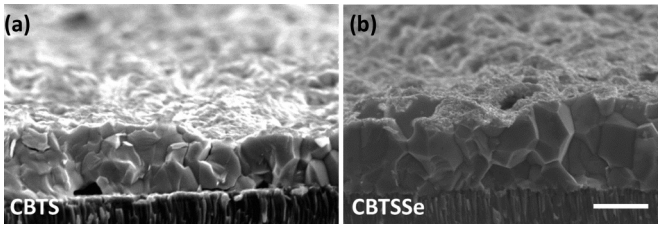

FIG. 8. SEM image of (a) CBTS and (b) CBTSSe films formed from a Cu_2SnS_3/BaS stack (scale bar, 1 μm).

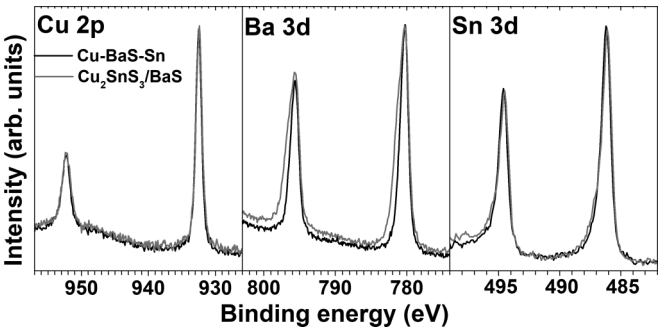

FIG. 9. XPS Al $K\alpha$ spectra of the Cu 2p, Ba 3d, and Sn 3d core levels of CBTS formed from co-sputter-deposited (black) and Cu_2SnS_3/BaS stacked (gray) films.

shoulders when compared to CBTS formed from co-sputter-deposited precursors. This indicates that a second species rich in Ba and Sn is present as a thin crust on the surface. While the chemical nature of the surface crust would require a detailed investigation to identify, the precursor films are briefly exposed to air between sputter deposition and annealing under S in a N_2-filled glovebox. Thus we cannot rule out an oxide species forming on the surface, which would be consistent with the observed shifts to higher binding energy.

IV. CONCLUSION

The phase evolution of co-sputter-deposited films of Cu-BaS-Sn were analyzed during formation using a combination of *in situ* and *ex situ* analyses via SEM, EDS, XRD, and EDXRD. It was found that migration of Cu to the surface during early stages of sulfurization (at temperatures as low as 250 °C) led to CBTS films exhibiting a two-layer morphology, with large grains at the top and small grains at the bottom, which carried over to the CBTSSe films during the subsequent selenization step (also leading to voiding at the back contact). The segregation could be reduced by extending the lower-temperature S anneal to long times (e.g., 3 h), although some remnant of this layering still remained even after these long treatments. The large surface-grain film structure could be extended to the full film thickness when Cu was placed on top of a BaS/Sn stacked precursor film prior to the heat treatment, presumably leading to a more localized nucleation of the CBTS/CBTSSe phase. However, it was found that neat bottom layers of BaS led to blister formation while forming BaS_3, and mitigating strategies should be considered when depositing stacked precursors. By binding the Cu to a ternary phase in the bulk of the film prior to conversion to CBTS, Cu migration could be alleviated, with the resulting films avoiding the two-layer morphology. This study underlies the importance of Cu migration on film structure during CBTS formation. Strategies to overcome multilayer formation should consider the rapid migration times of Cu and the relative thermodynamic stabilities of the different layers.

ACKNOWLEDGMENTS

This material is based upon work supported by the Duke University Energy Initiative Research Seed Fund. J.P.S. thanks the Natural Sciences and Engineering Research Council of Canada for a postdoctoral fellowship. The work was performed in part at the Duke University Shared Materials Instrumentation Facility (SMIF), a member of the North Carolina Research Triangle Nanotechnology Network (RTNN), which is supported by the National Science Foundation (Grant No. ECCS-1542015) as part of the National Nanotechnology Coordinated Infrastructure (NNCI). This research was partly supported by the H2020 program under the project STARCELL (H2020-NMBP-03-2016-720907) and by the Helmholtz Virtual Institute VI-520. Special thanks go to C. Hages, S. Levcenco, S. Schäfer, M. Klaus, and G. Wagener for their support during beamtime at BESSY II and to T. Unold for fruitful discussions.

[1] M. A. Green, Y. Hishikawa, W. Warta, E. D. Dunlop, D. H. Levi, J. Hohl-Ebinger, and A. W. H. Ho-Baillie, Prog. Photovoltaics **25**, 668 (2017).
[2] C. S. Tao, J. Jiang, and M. Tao, Sol. Energy Mater. Sol. Cells **95**, 3176 (2011).
[3] A. Feltrin and A. Freundlich, Renew. Energy **33**, 180 (2008).
[4] W. Wang, M. T. Winkler, O. Gunawan, T. Gokmen, T. K. Todorov, Y. Zhu, and D. B. Mitzi, Adv. Energy Mater. **4**, 1301465 (2014).
[5] T. Gokmen, O. Gunawan, T. K. Todorov, and D. B. Mitzi, Appl. Phys. Lett. **103**, 103506 (2013).
[6] G. Rey, G. Larramona, S. Bourdais, C. Choné, B. Delatouche, A. Jacob, G. Dennler, and S. Siebentritt, Sol. Energy Mater. Sol. Cells **179**, 142 (2018).
[7] M. Nishiwaki, K. Nagaya, M. Kato, S. Fujimoto, H. Tampo, T. Miyadera, M. Chikamatsu, H. Shibata, and H. Fujiwara, Phys. Rev. Mater. **2**, 085404 (2018).
[8] S. Levcenko, J. Just, A. Redinger, G. Larramona, S. Bourdais, G. Dennler, A. Jacob, and T. Unold, Phys. Rev. Appl. **5**, 024004 (2016).
[9] D. Shin, B. Saparov, T. Zhu, W. P. Huhn, V. Blum, and D. B. Mitzi, Chem. Mater. **28**, 4771 (2016).
[10] D. Shin, B. Saparov, and D. B. Mitzi, Adv. Energy Mater. **7**, 1602366 (2017).
[11] T. Zhu, W. P. Huhn, G. C. Wessler, D. Shin, B. Saparov, D. B. Mitzi, and V. Blum, Chem. Mater. **29**, 7868 (2017).
[12] F. Hong, W. Lin, W. Meng, and Y. Yan, Phys. Chem. Chem. Phys. **18**, 4828 (2016).
[13] Z. Xiao, W. Meng, J. V. Li, and Y. Yan, ACS Energy Lett. **2**, 29 (2017).
[14] R. D. Shannon, Acta Crystallogr. A **32**, 751 (1976).
[15] J. Ge, Y. Yu, and Y. Yan, ACS Energy Lett. **1**, 583 (2016).
[16] J. Ge, P. Koirala, C. R. Grice, P. J. Roland, Y. Yu, X. Tan, R. J. Ellingson, R. W. Collins, and Y. Yan, Adv. Energy Mater. **7**, 1601803 (2017).
[17] J. Ge and Y. Yan, J. Mater. Chem. C **5**, 6406 (2017).
[18] D. Shin, T. Zhu, X. Huang, O. Gunawan, V. Blum, and D. B. Mitzi, Adv. Mater. **29**, 1606945 (2017).
[19] Z. Chen, K. Sun, Z. Su, F. Liu, D. Tang, H. Xiao, L. Shi, L. Jiang, X. Hao, and Y. Lai, ACS Appl. Energy Mater. **1**, 3420 (2018).
[20] J. Ge, Y. Yu, and Y. Yan, J. Mater. Chem. A **4**, 18885 (2016).
[21] D. Shin, E. Ngaboyamahina, Y. Zhou, J. T. Glass, and D. B. Mitzi, J. Phys. Chem. Lett. **7**, 4554 (2016).
[22] J. Ge, P. J. Roland, P. Koirala, W. Meng, J. L. Young, R. Petersen, T. G. Deutsch, G. Teeter, R. J. Ellingson, R. W. Collins, and Y. Yan, Chem. Mater. **29**, 916 (2017).
[23] Y. Zhou, D. Shin, E. Ngaboyamahina, Q. Han, C. B. Parker, D. B. Mitzi, and J. T. Glass, ACS Energy Lett. **3**, 177 (2018).
[24] B. Teymur, Y. Zhou, E. Ngaboyamahina, J. T. Glass, and D. B. Mitzi, Chem. Mater. **30**, 6116 (2018).
[25] A. Nagoya, R. Asahi, R. Wahl, and G. Kresse, Phys. Rev. B **81**, 113202 (2010).

[26] A. Walsh, S. Chen, S.-H. Wei, and X.-G. Gong, Adv. Energy Mater. **2**, 400 (2012).
[27] S. Chen, A. Walsh, X.-G. Gong, and S.-H. Wei, Adv. Mater. **25**, 1522 (2013).
[28] H. Katagiri, K. Jimbo, M. Tahara, H. Araki, and K. Oishi, MRS Proc. **1165**, 1165 (2009).
[29] D. A. R. Barkhouse, O. Gunawan, T. Gokmen, T. K. Todorov, and D. B. Mitzi, Prog. Photovoltaics Res. Appl. **20**, 6 (2012).
[30] O. Gunawan, T. Gokmen, C. W. Warren, J. D. Cohen, T. K. Todorov, D. A. R. Barkhouse, S. Bag, J. Tang, B. Shin, and D. B. Mitzi, Appl. Phys. Lett. **100**, 253905 (2012).
[31] C. Genzel, I. A. Denks, R. Coelho, D. Thomas, R. Mainz, D. Apel, and M. Klaus, J. Strain Anal. Eng. Des. **46**, 615 (2011).
[32] U. Mueller, R. Förster, M. Hellmig, F. U. Huschmann, A. Kastner, P. Malecki, S. Pühringer, M. Röwer, K. Sparta, M. Steffien, M. Ühlein, P. Wilk, and M. S. Weiss, Eur. Phys. J. Plus **130**, 141 (2015).
[33] H. Rodriguez-Alvarez, I. M. Kötschau, and H. W. Schock, J. Cryst. Growth **310**, 3638 (2008).
[34] R. Mainz and R. Klenk, J. Appl. Phys. **109**, 123515 (2011).
[35] See Supplemental Material at http://link.aps.org/supplemental/10.1103/PhysRevMaterials.3.055402 for XPS spectra of co-sputter-deposited films at various annealing temperatures under sulfur; SEM images of CBTS formed from a BaS/Sn/Cu precursor stack.
[36] R. Mainz, B. C. Walker, S. S. Schmidt, O. Zander, A. Weber, H. Rodriguez-Alvarez, J. Just, M. Klaus, R. Agrawal, and T. Unold, Phys. Chem. Chem. Phys. **15**, 18281 (2013).
[37] N. J. Carter, R. Mainz, B. C. Walker, C. J. Hages, J. Just, M. Klaus, S. S. Schmidt, A. Weber, W.-C. D. Yang, O. Zander, E. A. Stach, T. Unold, and R. Agrawal, J. Mater. Chem. C **3**, 7128 (2015).
[38] A. Weber, S. Schmidt, D. Abou-Ras, P. Schubert-Bischoff, I. Denks, R. Mainz, and H. W. Schock, Appl. Phys. Lett. **95**, 041904 (2009).
[39] E. Simsek Sanli, Q. M. Ramasse, R. Mainz, A. Weber, D. Abou-Ras, W. Sigle, and P. A. van Aken, Appl. Phys. Lett. **111**, 032103 (2017).
[40] T. Petzel, Z. Für Anorg. Allg. Chem. **396**, 173 (1973).
[41] H. G. v. Schnering and N.-K. Goh, Naturwissenschaften **61**, 272 (1974).
[42] T. A. Bither, R. J. Bouchard, W. H. Cloud, P. C. Donohue, and W. J. Siemons, Inorg. Chem. **7**, 2208 (1968).